The effect of insoluble surfactant at dilute concentration on drop breakup under shear with inertia

M. A. Drumright-Clarke and Y. Renardy

Citation: Physics of Fluids (1994-present) **16**, 14 (2004); doi: 10.1063/1.1628232
View online: http://dx.doi.org/10.1063/1.1628232
View Table of Contents: http://scitation.aip.org/content/aip/journal/pof2/16/1?ver=pdfcov
Published by the AIP Publishing

The effect of insoluble surfactant at dilute concentration on drop breakup under shear with inertia

M. A. Drumright-Clarke
Southwest Research Institute, 6220 Culebra Road, San Antonio, Texas 78238-5166

Y. Renardy[a)]
Department of Mathematics and ICAM, 460 McBryde Hall, Virginia Tech, Blacksburg, Virginia 24061-0123

(Received 22 July 2002; accepted 15 September 2003; published online 13 November 2003)

Direct numerical simulations are conducted with a volume-of-fluid continuous surface stress algorithm. The linear equation of state is used to characterize the effects of an insoluble surfactant at low concentration on a drop in strong shear. The drop and the surrounding liquid have the same viscosity and density. Surfactant migration induces a Marangoni force that acts toward the drop center. For low inertia, viscous force opposes the Marangoni force, so that a stationary drop with surfactant is more elongated and less tilted than without. The addition of surfactant promotes breakup, lowering the critical capillary number. The first daughter drops are smaller than for the case of clean drops. For high inertia, the Marangoni force retracts the drop and retards breakup. The local values of surface tension are computed during drop evolution. © *2004 American Institute of Physics.* [DOI: 10.1063/1.1628232]

I. INTRODUCTION

We consider the effect of insoluble surfactants on drop deformation, breakup, and drop size distribution of daughter drops.[1–7] Previous numerical studies include the use of the boundary integral method for extensional Stokes flow, for a range of surfactant concentrations.[8–10] In particular, the nonlinear surface equation of state[9] accounts for surface saturation and nonideal interactions among the surfactant molecules, as well as the case of strong intersurfactant cohesion. These nonlinear terms are important even at moderate surface concentrations, but in the dilute case which we consider, the linear equation of state holds. Previous studies on the dilute case include numerical simulations of stationary drop shapes allowing for surfactant diffusion.[11,12] These concern zero Reynolds number. In this paper, we focus on critical conditions, breakup and satellite drop volumes at nonzero Reynolds number, and dependence on the introduction of a small amount of surfactant.

As a model problem, we study the case of equal viscosity μ and density ρ for the drop and surrounding matrix liquid. Direct numerical simulations are conducted with a three-dimensional volume-of-fluid continuous-surface-stress formulation (VOF-CSS). The components of our code SURFER++ are extensively described in Refs. 13–20 and we refer the reader to them. The initial shape is a spherical drop of radius a as shown in Fig. 1. The computational domain as shown is a box of size $L_x \times L_y \times L_z$. Periodicity is imposed in the x and y directions. Initially, the top and bottom walls are instantaneously set in motion and impose a constant shear rate $\dot{\gamma}$.

A rectangular Cartesian mesh is used for finite differences on a staggered grid.[21–27] The fluids are incompressible and governed by the Navier–Stokes equation:

$$\nabla \cdot \mathbf{u} = 0, \tag{1}$$

$$\rho\left(\frac{\partial \mathbf{u}}{\partial t} + \mathbf{u}\cdot\nabla\mathbf{u}\right) = -\nabla p + \nabla \cdot \mu\mathbf{S} + \mathbf{F}, \tag{2}$$

$$\mathbf{S}_{ij} = \frac{1}{2}\left(\frac{\partial u_j}{\partial x_i} + \frac{\partial u_i}{\partial x_j}\right), \tag{3}$$

where $\mathbf{u}$ denotes velocity and $\mathbf{F}$ denotes the body force. Fluid interfaces are constructed from the values of the volume-of-fluid (VOF) function $C(x,y,z)$:[27]

$$C(x,y,z) = \begin{cases} 1 & \text{for matrix fluid,} \\ 0 & \text{for drop fluid.} \end{cases} \tag{4}$$

When discretized, C represents the volume fraction of the matrix fluid in each grid cell. The VOF function is transported with a Lagrangian advection scheme using the velocity field computed at each time step. From the values of C at each time step, the interface is reconstructed with the piecewise linear interface reconstruction (PLIC) method.[24] The time integration is performed with a semi-implicit scheme to handle low Reynolds numbers.[17] On the cells which contain the interface, the interfacial tension force $\mathbf{F_s}$ is part of the body force $\mathbf{F}$ in (2):[21]

$$\mathbf{F_s} = \nabla \cdot \mathbf{T}, \quad \mathbf{T} = [(\mathbf{1} - \mathbf{n_S} \otimes \mathbf{n_S})\sigma_e \delta_S], \tag{5}$$

where σ_e denotes the coefficient of surface tension, κ is the mean curvature, $\mathbf{n_S}$ is the normal to the surface, and δ_S is a delta function concentrated on the interface. Over each cell, gravitational force is included in the body force term.

The formulation for the linear equation of state for surfactants within the VOF-CSS framework is described in detail in Ref. 28. This reference documents the performance of

a)Author to whom correspondence should be addressed. Telephone: (540) 231-8258; electronic mail: renardyy@math.vt.edu

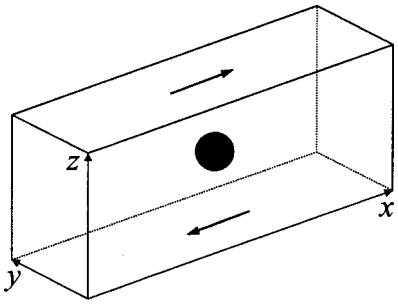

FIG. 1. Sketch of the initial condition. A drop is suspended in a matrix liquid, and subjected to simple shear generated by the motion of the top and bottom walls.

the algorithm for drop deformation at low viscosity ratio. Briefly, in the VOF scheme, properties of the fluid are identified with volumes rather than surfaces; i.e., the surfactant layer is represented as the region between two volumes. As part of the initial condition (Fig. 1), we define two additional spheres, one interior to the drop with radius $h/2$ smaller, and one exterior to the drop with radius $h/2$ larger, where h is sufficiently small compared with the mesh size. Figure 2 illustrates the initial surfactant distribution, in which the surface of the drop is encased in a surfactant layer. The three interfaces are tracked during the numerical simulation.

At the continuous level, the outer sphere is defined by a VOF function c_+ which is 1 inside it and 0 outside. The inner sphere is defined by c_-, which is 1 inside it and 0 outside. Surfactant concentration Γ is then a constant multiple of $c_+ - c_-$, which is 1 within the annular region, and 0 elsewhere. Initially, the surfactant is evenly distributed on the interface, and therefore the effective surface tension in (5) is

$$\sigma_e = \sigma - E\Gamma = \sigma(1-r), \tag{6}$$

where the elasticity number E measures the sensitivity of the surface tension to the surfactant concentration Γ,[8] σ denotes the surface tension coefficient without surfactant, and r is defined as the reduction factor:

$$r = E\Gamma/\sigma. \tag{7}$$

The linear equation of state changes (5) to

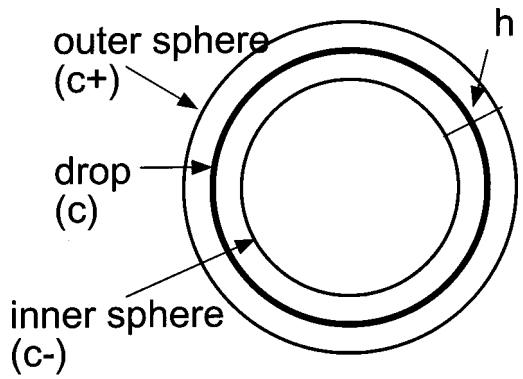

FIG. 2. Sketch of initial surfactant layer. Three surfaces are defined with three separate volume fraction functions. The surfactant initially resides in the annulus between the inner and outer spheres.

$$\mathbf{T} = (\mathbf{1} - \mathbf{n}_S \otimes \mathbf{n}_S)\left[\sigma|\nabla C| - \frac{r\sigma}{h}(c_+ - c_-)\right]. \tag{8}$$

Here, note that δ_s in (5) is the same as $|\nabla C|$, and integrates to 1 across the interface. Analogously, in (8), the integral over the annulus of $|\nabla C|$ is

$$\int_{a-(h/2)}^{a+(h/2)} -\frac{\partial C}{\partial r}\,dr = -c_+ + c_- = 1. \tag{9}$$

The integral of the next term $(r\sigma/h)(c_+ - c_-)$ across the annulus of width h yields σr, which by (6) and (7), gives $E\Gamma$. This confirms that (8) represents the modification $\sigma_e \rightarrow \sigma - E\Gamma$.

To reconstruct surfactant concentrations, we need to divide the amount of surfactant by surface area. The VOF formulation produces an amount of surfactant within a grid cell, i.e., a volume, and it does not directly give a surface area. We obtain an estimate of surface area by reconstructing a planar interface which has the correct volume fraction and normal, and then computing the surface area of this planar interface within the given grid cell. To compute the normal, we use the gradient of a smoothed color function. We then obtain a surfactant concentration by dividing the surfactant amount within the cell by the surface area. To ensure that the surfactant stays within interface cells, we chose a small value for the initial thickness h of the surfactant layer. In some ''bad'' cells, however, there can be significant errors in surface area from the linear interface reconstruction. For instance, consider a spherical cap protruding slightly into a grid cell through one of its faces. If the direction of the surface normal is parallel to one of the coordinate axes, the calculated surface area will always be the full area of the cross section of the cell regardless of what the actual area is. Poor approximations of normals and surface areas in certain cells explain the rings observed on the plots of surfactant concentration. In future work, we expect to include surfactants in our PROST code,[19] which uses a quadratic surface reconstruction that should avoid some of these problems.

II. DIMENSIONLESS PARAMETERS

A flow in simple shear $\dot{x} = \dot{\gamma} z$, and $\dot{z} = 0$, where $\dot{} \equiv d/dt$, can be written as

$$\dot{\mathbf{x}} = \frac{\dot{\gamma}}{2}(\mathbf{S} + \mathbf{A})\dot{\mathbf{x}}, \tag{10}$$

$$\mathbf{S} = \begin{pmatrix} 0 & 1 \\ 1 & 0 \end{pmatrix}, \quad \mathbf{A} = \begin{pmatrix} 0 & 1 \\ -1 & 0 \end{pmatrix}, \quad \mathbf{x} = \begin{pmatrix} x \\ z \end{pmatrix}. \tag{11}$$

The motion generated by the symmetric matrix $\mathbf{S}$, $\dot{\mathbf{x}} = \mathbf{S}\mathbf{x}$, is an elongation at an angle of 45° to the flow direction, while the motion generated by the antisymmetric matrix $\mathbf{A}$, $\dot{\mathbf{x}} = \mathbf{A}\mathbf{x}$, is pure rotation. When a drop is placed in this flowfield, viscous shear initially stretches it at that angle of tilt, and a rotational motion develops inside. A stationary shape in Stokes flow occurs when the deforming viscous force $\sim \mu\dot{\gamma}$ is much less than the restoring surface-tension force $\sim \sigma/a$, while the reverse leads to fragmentation. This competition is parametrized by the capillary number

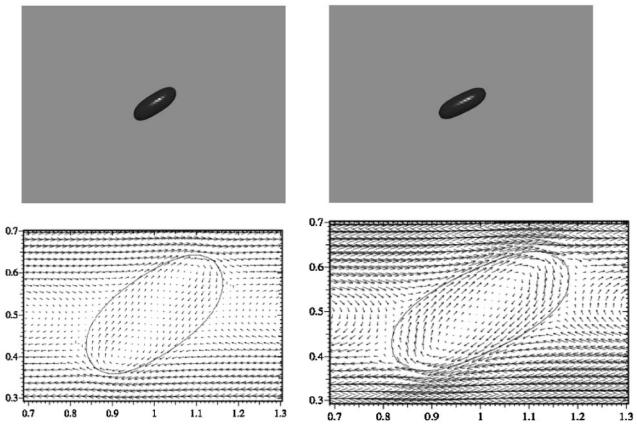

FIG. 3. Comparison of stationary drop shapes with maximal elongation for Re=10. $r=0$ (left, Ca=0.15) and $r=0.1$ (right, $\mathrm{Ca}_e=0.14$). Velocity vectors are shown in the $x-z$ cross section through the center of the drop.

$$\mathrm{Ca}=\mu\dot{\gamma}a/\sigma. \tag{12}$$

For Stokes flow with matching viscosity and density, the critical capillary number is 0.43.[1,3,5,29–31]

A Reynolds number,

$$\mathrm{Re}=\rho\dot{\gamma}a^2/\mu, \tag{13}$$

measures the inertial vs viscous effects. Renardy *et al.* show in Refs. 28, 32, 33 that inertia breaks up a clean drop at a lower capillary number than in Stokes flow. At large Re, a drop breaks when the Reynolds stress which is order $\rho|\mathbf{v}|^2=\rho\dot{\gamma}^2a^2$ competes with capillary stress of order σ/a. This critical condition is, upon division by the viscous stress $\mu\dot{\gamma}$, $\mathrm{Re}_c\sim 1/\mathrm{Ca}_c$. This is better expressed in terms of the Weber number We=ReCa which is the ratio of inertial to capillary forces:

$$\mathrm{We}_c\sim 1, \quad \text{at large Re}. \tag{14}$$

Supportive numerical evidence is given in Ref. 32.

In order to compare the behaviors of a clean drop vs a surfactant laden drop at reduction r, we define an "effective" capillary number:

$$\mathrm{Ca}_e=\frac{a\dot{\gamma}\mu_m}{\sigma_e}=\frac{\mathrm{Ca}}{1-r}. \tag{15}$$

With this definition, the drops may be expected to behave in the same way at the same effective capillary number if the surfact were to remain evenly distributed over the interface. Any differences in evolution for drops at the same Ca_e are due to migration of the surfactant, which we study next.

III. SURFACTANT MIGRATION

In this section, the case Re=10 is investigated in detail. Figure 3 provides a comparison of stationary shapes for a clean drop (left, Ca=0.15) and reduction factor 0.1 (right, $\mathrm{Ca}_e=0.14$). These shapes are not sensitive to small changes in the capillary numbers below the critical value. The velocity vector plot for the clean drop shows a more complicated flow structure than the single swirl inside the surfactant-laden drop.

Figure 4 shows how surface tension values change over the drop in response to the flowfield. The colorbar shows the range of reduction factor: surface tension in the lightest areas has been reduced by 30% or more. The surfactant accumulates at the low velocity areas or "dead spots" at the top front and bottom back of the drop, which eventually have minimal surface tension. This accumulation of surfactant at the ends generates a Marangoni stress[9] in the shear stress balance at the interface:

$$\mathrm{Ma}=\frac{\partial\sigma}{\partial\Gamma}\nabla_S\Gamma. \tag{16}$$

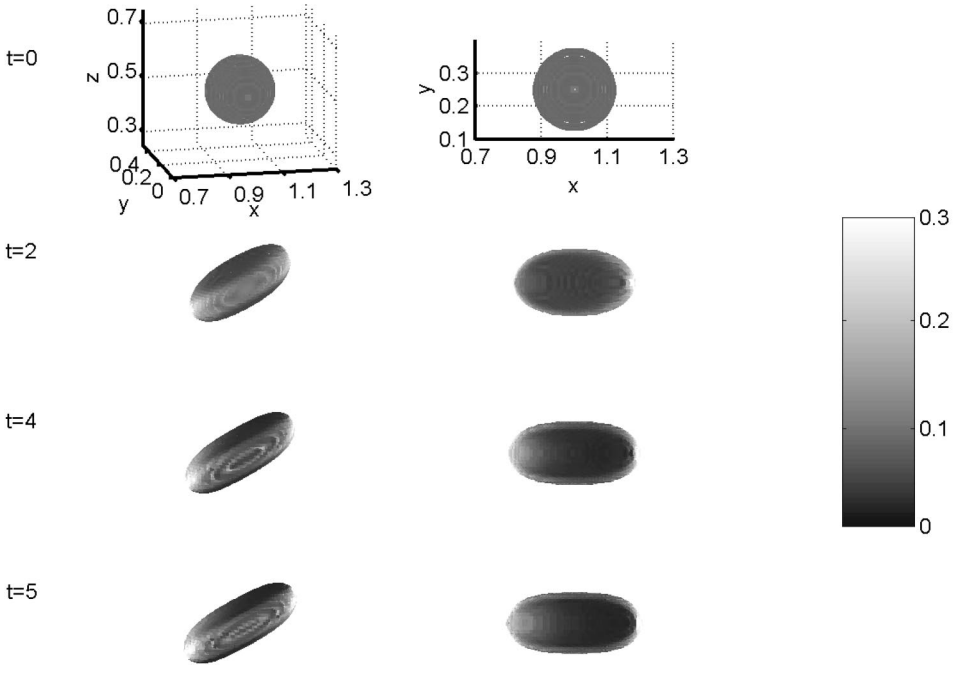

FIG. 4. Re=10, $\mathrm{Ca}_e=0.14$, $r=0.1$. Quantitative values of surface tension are shown for dimensionless times 0, $2\dot{\gamma}^{-1}$, $4\dot{\gamma}^{-1}$, $5\dot{\gamma}^{-1}$. The shading shows the reduction factor r from 0 (Ca=0.13) to 0.3 (30% reduction in surface tension). Down the first column, the drop is viewed in 3D with axes shown at the initial time. The second column shows the view from above the drop. A stationary shape is attained by dimensionless time $5\dot{\gamma}^{-1}$.

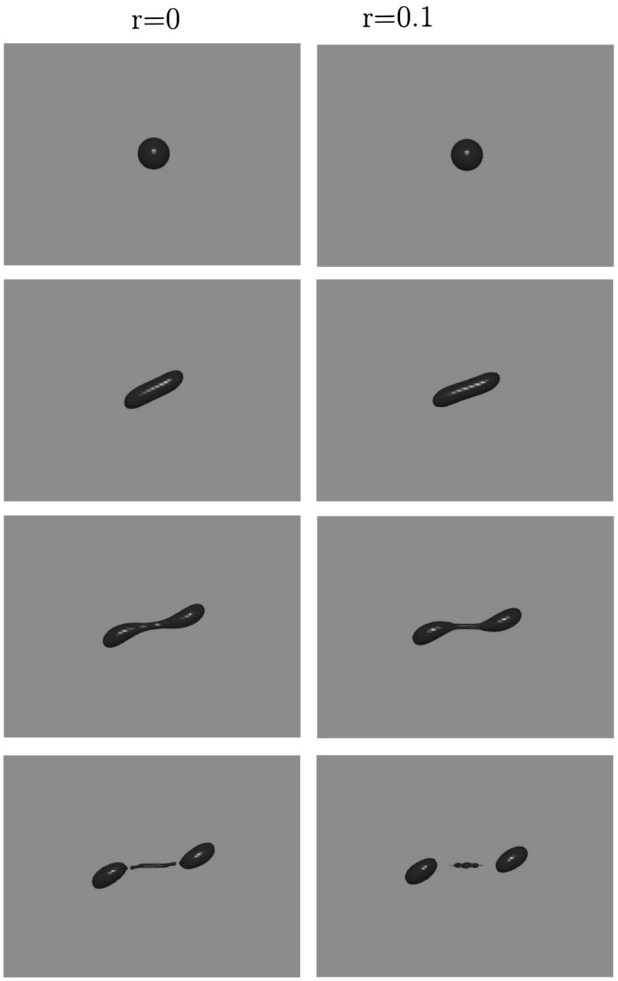

FIG. 5. Comparison of drop shapes with and without surfactant at Re=10. $r=0$ (left column), and $r=0.1$ (right), $\mathrm{Ca}_e=0.15$. $t=0$, 10, 22, $24\dot{\gamma}^{-1}$.

In regions where surface tension changes rapidly, the Marangoni stress sets up a local flow opposite to surfactant migration. The Marangoni force is therefore directed toward the drop center, and significant near the top of the front end cap and the bottom of the back end cap. This combination decreases the tilt. It also enhances retraction; however, surface tension at the end caps is small, so that the interior flow pushes the interface outward and contributes to drop elongation.

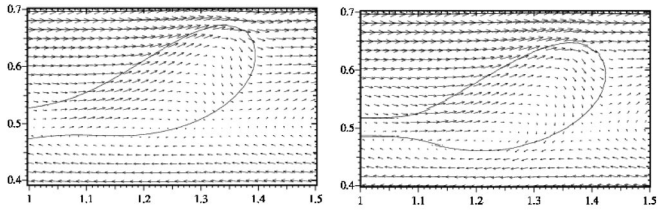

FIG. 7. Vector velocity plots of break-up area corresponding to Fig. 6 at $t=23\dot{\gamma}^{-1}$. $r=0$ (left), 0.1 (right).

Figures 5 and 6 show a breakup sequence. In Fig. 5, both the clean (left) and surfactant-laden (right) drops break at roughly the same effective capillary number $\mathrm{Ca}_e\approx 0.15$. Just as in the stationary case of Fig. 3, the drop with surfactant elongates more and the angle of inclination is lower.

Figure 6 shows quantitative values of surface tension for the surfactant-laden drop. By $t=17\dot{\gamma}^{-1}$, surface tension is higher in the middle of the drop. Hence, the capillary force which controls the pinching process, is stronger for the middle portion of the surfactant-laden drop than for the clean drop. Contraction and pinch-off are therefore promoted by surfactant.

Figure 7 is a comparison of velocities in the $x-z$ plane across the dumbbells for the clean and surfactant-laden drops at $t=23\dot{\gamma}^{-1}$. The front dumbbell for the surfactant-laden drop bulges slightly at the bottom, into a velocity field that is directed toward the back dumbbell. The surfactant at what used to be a dead spot (lower front end) is advected toward the middle of the drop; e.g., at $t=22\dot{\gamma}^{-1}$ in Fig. 6. The Marangoni force at the top of the dumbbell at $t=22\dot{\gamma}^{-1}$ points toward the neck, and at the bottom of this dumbbell, points away from the neck, stalling the swirling motion inside the dumbbell. After the daughter drops detach, the ef-

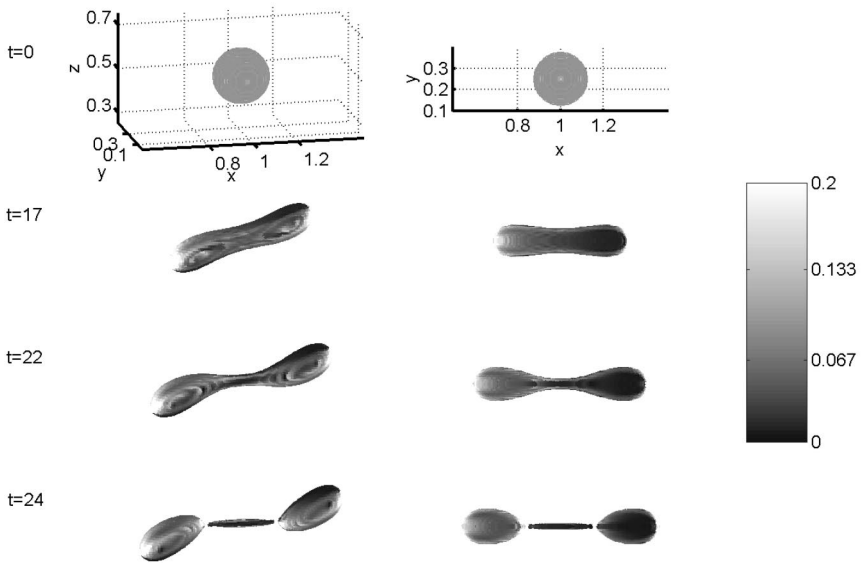

FIG. 6. Re=10, $\mathrm{Ca}_e=0.15$, $r=0.1$. Quantitative values of reduction factor r are shown for dimensionless times 0, 17, 22, $24\dot{\gamma}^{-1}$. r varies from 0 ($\mathrm{Ca}=0.14$) to 0.2 (20% reduction in surface tension). Down the first column, the drop is viewed in 3D with axes shown at the initial time. The second column shows the view from above.

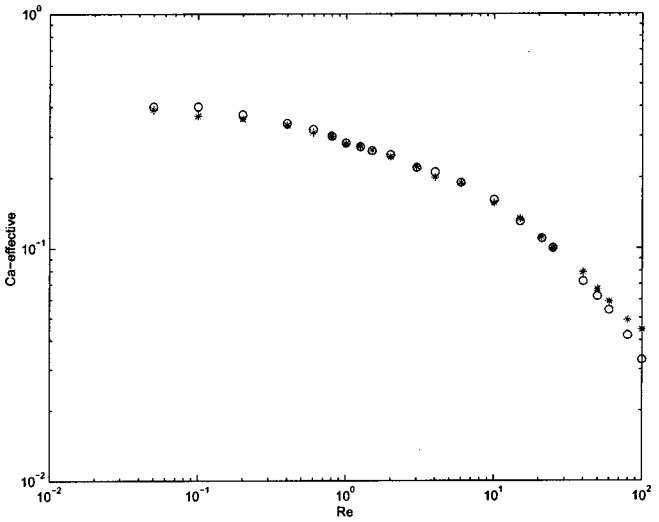

FIG. 8. Critical conditions for Re vs Ca_e. $r=0$ (○) and $r=0.1$ (∗). The drop and matrix liquids have equal viscosity and equal density.

fective surface tension at the central filament in Fig. 6 is lower for the surfactant-laden drop.

IV. CRITICAL CURVES

Critical conditions for the clean (○) and reduction 0.1 (∗) drops are plotted in Fig. 8 for Ca_e vs Re. There is a crossover around Re≈40, below which surfactant promotes breakup and above which it retards it. The crossover is a result of the competition between viscous force which generates a shear stress at the interface, and inertial force which does not. In Sec. III for the case Re=10, we see that the viscous force, together with the decrease in surface tension at the ends, promotes elongation. Beyond the crossover point, the viscous force becomes insignificant, so that the Marangoni force is unopposed.

Table I shows how the properties of stationary drops vary with Re. L/a denotes maximal half-length/radius and θ denotes the angle of inclination with the horizontal. For this table, surfactant is added to the level of $r=0.1$ while keeping other fluid parameters the same. At higher levels of reduction with the linear equation of state, there is little difference in the physical nature of breakup, which occurs at similar effective capillary numbers.[34]

As Re increases, another effect that is present in both the clean and surfactant-laden drops is that the tilt angle increases: compare Figs. 3 and 5 at Re=10 with Figs. 9 and 10 for Re=50. When inertia is important in the matrix liquid,

TABLE I. At each Re, maximal L/a and angle of tilt θ for stationary shapes are compared for a clean drop (left) and with surfactant ($r=0.1$, right).

	$r=0$			$r=0.1$		
Re	Ca	L/a	θ(°)	Ca_e	L/a	θ (°)
1.0	0.27	1.8	28	0.27	2.1	26
2.0	0.24	1.8	28	0.23	1.9	26
3.0	0.21	1.7	33	0.21	1.8	26
10.0	0.15	1.6	35	0.14	1.6	30
50.0	0.061	1.5	48	0.062	1.5	42

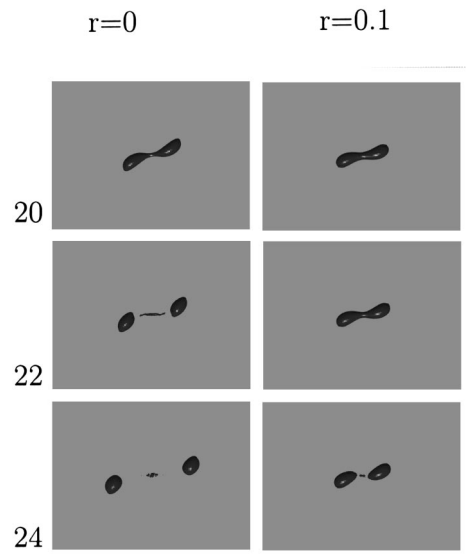

FIG. 9. Comparison of drop shape with and without surfactant when inertia is important. Re=50, $r=0$, Ca=0.060 (left) and $r=0.1$, $Ca_e=0.066$ (right). $t=20,\ 22,\ 24\dot{\gamma}^{-1}$.

Bernoulli's equation yields that $p+\rho|\mathbf{v}|^2/2$ is constant along each streamline. Therefore, the large velocities near the tips induce negative pressures relative to elsewhere. The resulting suction leads to higher tilting of the drop. The higher tilt induces secondary centers of circulation. For the surfactant-laden drop, the Marangoni force at Re=60 retards the rotational motion in the interior to a level similar to the clean drop at Re=10.

V. EFFECT OF SURFACTANT ON DAUGHTER DROP VOLUMES

Shear-mixing typically results in drops of various sizes, and information on drop size distribution is helpful in determining the mechanical properties of the blend.[7] In this section, we examine the effect of surfactant on the size of the first daughter drops. We consider a situation in which the fluid properties and flow strength are fixed, while the mother drop size is increased. Once the size increases over a critical volume, breakup ensues. Only the initial radius a is varied; thus, the capillary and Reynolds numbers of the mother drop satisfy

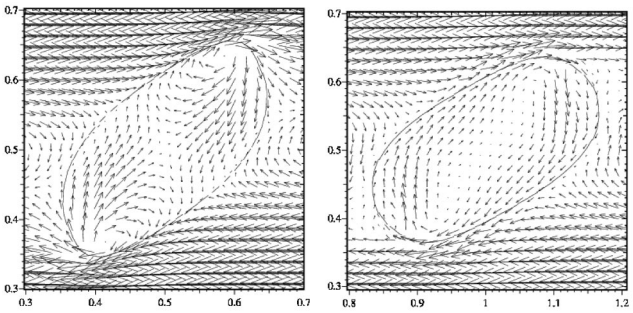

FIG. 10. Velocity vector plots in the $x-z$ plane through the centers of the drops for stationary shapes at Re=60. The clean drop (left) contains a more complicated circulation pattern compared to $r=0.1$ (right).

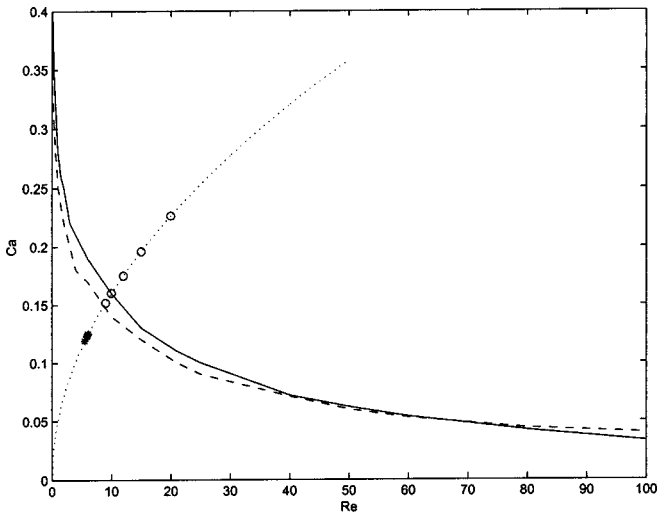

FIG. 11. Re vs Ca for critical curves at $r=0$ (solid), $r=0.1$ (dashed); Re $=391*\mathrm{Ca}^2$, fluid properties and flow strength fixed, radius of mother drop varies. Circles represent mother drops for Re=9, Ca=0.15; Re=10, Ca =0.16; Re=12, Ca=0.175; Re=15, Ca=0.20; Re=20, Ca=0.23. Asterisks represent daughter drops.

$$\mathrm{Re}/\mathrm{Ca}^2=K, \quad K=\rho\sigma^2/\mu^3\dot{\gamma}=\text{fixed}. \tag{17}$$

Viewed in the Ca vs Re plane, this curve is a parabola that intersects the critical curve at one point. That point defines the size at which the mother drop breaks. Figure 11 shows such a parabola (dotted) for $K=391$, together with the critical curve (dash) for reduction 0.1. The case of a clean drop is investigated in Ref. 33 and the solid line is for this case. Moving up the parabola from criticality, the first daughter drops of radius D are characterized by

$$\mathrm{Re}_D=\mathrm{Re}(D^2/a^2), \quad \mathrm{Ca}_D=(D/a)\mathrm{Ca}. \tag{18}$$

The circles along the parabola represent different volumes for the surfactant-laden mother drop. The asterisks on the parabola below criticality represent the first daughter drops. As for the clean drop when the mother volume is

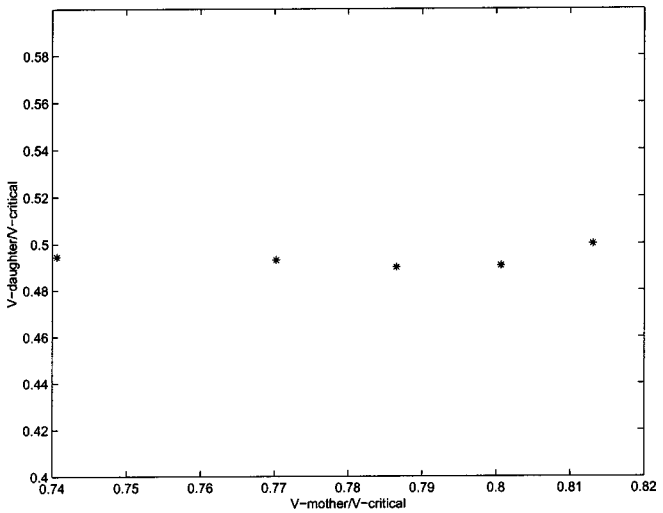

FIG. 12. Ratio of daughter volume to critical volume as the mother drop size increases saturates to roughly 50% of the critical volume. Mother drops are those of Fig. 11.

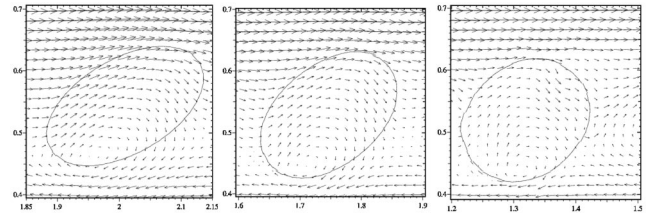

$Re=1,\ Ca_D=0.19$ $Re=10,\ Ca_D=0.11$ $Re=100,\ Ca_D=0.032$

FIG. 13. Velocity vector plots in the $x-z$ plane through the midsection of the first daughter drops. Re=1, 10, 100 just after pinch-off, corresponding to the case $r=0.1$ in Fig. 8.

increased, the first daughters of the surfactant-laden drop converge in volume to a certain fraction of the critical volume.

Figure 12 shows this behavior more clearly by focusing on the daughter volumes relative to the critical drop. Surfactant migration is similar to that of Fig. 6. With increase in the mother drop size, the daughters saturate to roughly 50% of the critical volume, the remaining volume going to the central neck. Compared to this, Ref. 33 finds that for a clean drop, the first daughters converge to roughly 60% of the critical volume.

When more surfactant is added, the rotational motion in the daughters at $r=0.1$ in Fig. 13 damps out. Figure 14 shows that the $r=0.2$ case has less circulation inside the daughter drop than at $r=0.1$. With further increase in reduction, the flow inside the daughter drop aligns with the exterior shear flow. This is because the viscosity and density of the drop and matrix liquids are the same, and with little surface tension, the daughter drop floats along with the matrix liquid.

VI. NUMERICAL ACCURACY

Numerical convergence for a breakup sequence with mesh, timestep and computational domain sizes are verified at Re=10, $\mathrm{Ca}_e=0.155$, $r=0.1$. The thickness of the surfactant layer is chosen $\frac{1}{100}\Delta x$ for a uniform numerical mesh: $\Delta x=\Delta y=\Delta z$. Spatial refinements for $\Delta x=a/12$ and $a/8$ agree, where a is the initial radius, so that the latter refinement is chosen for the bulk of the computations. The timestep is chosen $\Delta t=10^{-3}\dot{\gamma}^{-1}$, since a refinement of 1/10 of this retrieves identical results: daughter Reynolds number

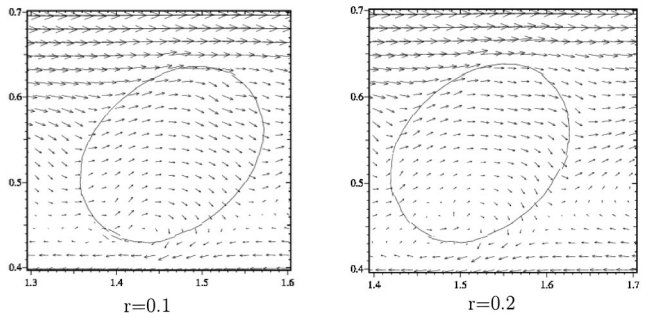

FIG. 14. Velocity vector plots in the $x-z$ plane through the midsection of first daughter drops, Re=60; $r=0.1$ ($\mathrm{Ca}_D=0.043$), 0.2 ($\mathrm{Ca}_D=0.033$).

and capillary number are converge to $\mathrm{Re}_D=6.2$, $\mathrm{Ca}_D=0.1$. Results for the computational domains $L_x=16a$ and $24a$ at $L_y=4a$, $L_z=8a$, show that the former suffices at $\mathrm{Re}=10$. However, the L_x decreases with Reynolds number because the drop shortens with inertia. For $\mathrm{Re}\leqslant 1.5$, the $L_x=24a$. For $\mathrm{Re}>1.5$, $L_x=16a$. The different computational domain sizes are chosen to minimize interference between neighboring drops.

VII. CONCLUSION

Surface tension is computed for surfactant-laden drops that evolve to stationary states and those that end-pinch close to critical capillary numbers. The density and viscosity of the drop and matrix liquids are the same. The case of the reduction factor 0.1 is studied in detail.

The viscous force in the matrix liquid sweeps the surfactant toward the end caps. Surface tension decreases locally there, allowing the rotational motion inside the drop to push the interface out. For example, at $\mathrm{Re}=10$, this leads to more elongation than achieved by a clean drop at the same effective capillary number. Marangoni force acts to lower the angle of tilt. For capillary numbers that lead to drop breakup, surface tension at the neck eventually becomes higher than for the clean drop, and end-pinching occurs earlier for the surfactant-laden drop. The addition of a small amount of surfactant decreases daughter drop volumes relative to the critical volume. For Re below approximately 40, the critical effective capillary number for the surfactant-laden drop is below that for a clean drop. For higher Re, the reverse occurs. For matched Reynolds number and effective capillary number, breakup times are reduced when more surfactant is added.

For Re over 40, inertial force becomes significant, and the angle of tilt increases for both the clean and surfactant-laden drops. The viscous force that would elongate the drop is small. For the surfactant-laden drop, the Marangoni force retards elongation, and also retards the rotational motion inside the drop to a less complicated circulation pattern compared with the clean drop at the same effective capillary number.

ACKNOWLEDGMENTS

This research was sponsored by NSF-INT 9815106, NSF-DMS SCREMS, NSF-CTS 0090381, and utilized the NCSA SGI Origin 2000. Acknowledgement is made to the donors of The Petroleum Research Fund, administered by the ACS, for support of this research. We thank Michael Renardy for discussions, and Stephane Zaleski and Jie Li for SURFER.

[1] J. M. Rallison, "The deformation of small viscous drops and bubbles in shear flows," Annu. Rev. Fluid Mech. **16**, 45 (1984).
[2] R. A. De Bruijn, "Tipstreaming of drops in simple shear flows," Chem. Eng. Sci. **48**, 277 (1993).
[3] H. A. Stone, "Dynamics of drop deformation and breakup in viscous fluids," Annu. Rev. Fluid Mech. **26**, 65 (1994).
[4] S. Guido and M. Villone, "Three-dimensional shape of a drop under simple shear flow," J. Rheol. **42**, 395 (1998).
[5] C. R. Marks, "Drop breakup and deformation in sudden onset strong flows," Ph.D. thesis, University of Maryland at College Park, 1998.
[6] S. Wannaborworn, "The deformation and breakup of viscous droplets in immiscible liquid systems for steady and oscillatory shear," Ph.D. thesis, University of Cambridge, Department of Chemical Engineering, 2001.
[7] D. I. Bigio, C. R. Marks, and R. V. Calabrese, "Predicting drop breakup in complex flows from model flow experiments," Int. Polym. Proc. **XIII2**, 192 (1998).
[8] C. D. Eggleton, Y. P. Pawar, and K. J. Stebe, "Insoluble surfactants on a drop in an extensional flow: A generalization of the stagnated surface limit to deforming interfaces," J. Fluid Mech. **385**, 79 (1999).
[9] Y. P. Pawar and K. J. Stebe, "Marangoni effects on drop deformation in an extensional flow: The role of surfactant physical chemistry. I. Insoluble surfactants," Phys. Fluids **8**, 1738 (1996).
[10] W. J. Milliken, H. A. Stone, and L. G. Leal, "The effect of surfactant on the transient motion of Newtonian drops," Phys. Fluids A **5**, 69 (1993).
[11] X. Li and C. Pozrikidis, "The effects of surfactants on drop deformation and on the rheology of dilute emulsions in Stokes flow," J. Fluid Mech. **341**, 165 (1997).
[12] S. Yon and C. Pozrikidis, "A finite-volume/boundary-element method for flow past interfaces in the presence of surfactants, with application to shear flow past a viscous drop," Comput. Fluids **27**, 879 (1998).
[13] J. Li and Y. Renardy, "Direct simulation of unsteady axisymmetric core-annular flow with high viscosity ratio," J. Fluid Mech. **391**, 123 (1999).
[14] J. Li, Y. Renardy, and M. Renardy, "A numerical study of periodic disturbances on two-layer Couette flow," Phys. Fluids **10**, 3056 (1998).
[15] Y. Renardy and J. Li, "Comment on 'A numerical study of periodic disturbances on two-layer Couette flow' [Phys. Fluids **10**, 3056 (1998)]," **11**, 3189 (1999).
[16] J. Li and Y. Renardy, "Shear-induced rupturing of a viscous drop in a Bingham liquid," J. Non-Newtonian Fluid Mech. **95**, 235 (2000).
[17] J. Li, Y. Renardy, and M. Renardy, "Numerical simulation of breakup of a viscous drop in simple shear flow through a volume-of-fluid method," Phys. Fluids **12**, 269 (2000).
[18] J. Li and Y. Renardy, "Numerical study of flows of two immiscible liquids at low Reynolds number," SIAM Rev. **42**, 417 (2000).
[19] Y. Renardy and M. Renardy, "PROST: A parabolic reconstruction of surface tension for the volume-of-fluid method," J. Comput. Phys. **183**, 400 (2002).
[20] Y. Renardy, "Direct simulation of drop fragmentation under simple shear," in *Interfacial Fluid Dynamics and Transport Processes*, edited by R. Narayanan and D. Schwabe, Lecture Notes in Physics (Springer-Verlag, Berlin, 2003), pp. 305–325.
[21] B. Lafaurie, C. Nardone, R. Scardovelli, S. Zaleski, and G. Zanetti, "Modelling merging and fragmentation in multiphase flows with SURFER," J. Comput. Phys. **113**, 134 (1994).
[22] S. Zaleski, J. Li, and S. Succi, "Two-dimensional Navier–Stokes simulation of deformation and break-up of liquid patches," Phys. Rev. Lett. **75**, 244 (1995).
[23] S. Zaleski, J. Li, R. Scardovelli, and G. Zanetti, "Flows with interfaces: Dealing with surface tension and reconnection," in *Proceedings of the IMACS-COST Conference on Computational Fluid Dynamics* (International Association for Mathematics and Computers in Simulation, Lausanne, Switzerland, 1995), p. 53.
[24] J. Li, "Calcul d'Interface Affine par Morceaux (Piecewise Linear Interface Calculation)," C. R. Acad. Sci., Ser. IIb: Mec., Phys., Chim., Astron. **320**, 391 (1995).
[25] J. Li, "Résolution numérique de l'équation de Navier–Stokes avec reconnexion d'interfaces: Méthode de suivi de volume et application à l'atomisation," Ph.D. thesis, Université Pierre et Marie Curie, 1996.
[26] D. Gueyffier, J. Li, A. Nadim, R. Scardovelli, and S. Zaleski, "Volume-of-fluid interface tracking and smoothed surface stress methods for three-dimensional flows," J. Comput. Phys. **152**, 423 (1999).
[27] R. Scardovelli and S. Zaleski, "Direct numerical simulation of free surface and interfacial flow," Annu. Rev. Fluid Mech. **31**, 567 (1999).
[28] Y. Renardy, M. Renardy, and V. Cristini, "A new volume-of-fluid formulation for surfactants and simulations of drop deformation under shear at a low viscosity ratio," Eur. J. Mech. B/Fluids **21**, 49 (2002).
[29] V. Cristini, J. Blawzdziewicz, and M. Loewenberg, "Drop breakup in three-dimensional viscous flows," Phys. Fluids **10**, 1781 (1998).
[30] V. Cristini, "Drop dynamics in viscous flow," Ph.D. thesis, Yale University, 2000.

[31]J. Blawzdziewicz, V. Cristini, and M. Loewenberg, ''Critical behavior of drops in linear flows. I. Phenomenological theory for drop dynamics near critical stationary states,'' Phys. Fluids **14**, 2709 (2002).
[32]Y. Renardy and V. Cristini, ''Effect of inertia on drop breakup under shear,'' Phys. Fluids **13**, 7 (2001).
[33]Y. Renardy and V. Cristini, ''Scalings for fragments produced from drop breakup in shear flow with inertia,'' Phys. Fluids **13**, 2161 (2001).
[34]M. A. Drumright-Clarke, ''Numerical simulations that characterize the effects of surfactant on droplets in shear flow,'' Ph.D. thesis, Mathematics, Virginia Tech, 2002.